Detached Eddy Simulation of Restricted Shock Separated Flow in a Thrust Optimized Contoured Nozzle

A. SHAMS, P. COMTE & S. GIRARD

Laboratoire d'Etude Aérodynamiques (LEA), Université de Poitiers, ENSMA, CNRS
CEAT, 43 route de l'Aérodrome, F-86036 Poitiers, France

Résumé :

Cette étude présente la simulation numérique tridimensionnelle du décollement restrient du choc dans une tuyère à poussée optimisée. Cet écoulement acceléré est complexe, se produit à haute vitesse et contient de très fortes interactions choc-couche limite et de larges zones de décollement. Une nouvelle version de la DES (Detached Eddy Simulation) basée sur un modèle à deux équations ($k-\omega$) a été utilisée qui s'avère bien adaptée à ce type d'interaction. De plus, pour la discrétisation spatiale, un schéma à préservation de la monotonicité pondérée et essentiellement non-oscillatoire (MPWENO) du cinquième ordre a été utilisée pour résoudre les différentes discontinuités apparaîssant dans ce type d'écoulement.

Abstract :

This paper presents three dimensional numerical investigation of restricted shock separated (RSS) flow in a thrust optimized contoured nozzle. This type of complex high speed accelerating flow exhibits strong shock wave / boundary layer interaction and massive separation. A new version of detached-eddy simulation (DES) based on two-equation $k-\omega$ model has been used which deals very well with this type of interactions. In addition for space discretization a fifth order monotonicity preserving weighted essentially non-oscillatory (MPWENO) scheme has been used to capture different flow discontinuities appears in this complicated flow configuration.

Mots clefs : restricted shock separation, nozzle, detached-eddy simulation, MPWENO scheme

1 Introduction

Flow separation takes place in the rocket nozzles when it operates under overexpanded condition. This flow separation is undesirable due to its unsteady and non-symmetric nature. It causes dangerous unsteady lateral forces, so-called side loads which may cause structure damage. Past research have made it clear that depending upon nozzle contour two types of flow separation takes place, namely free shock separation (FSS) and restricted shock separation (RSS) [1]. A number of experimental, theoretical and numerical studies in the past have been performed to understand these flow separations [1]-[8]. Especially the origin of the side-load appears during these flow separations. Meanwhile it has been proven that in thrust-optimized contoured (TOC) nozzles, a major side-load occurs as a result of transition of separation pattern from free shock separation to the restricted shock separation (FSS to RSS) [3]. Apart from large side-loads high thermal stress on the nozzle wall can be generated during the transient of the operation by nonaxisymmetric behaviour of the separation line and the reattachment of the separated flow. Reasons for the transition between the separation patterns are discussed by Hagemann et al. [4] and have identified the cap-shock pattern to be the main cause of this transition. Previous studies concerning numerical simulations of the RSS regimes in TOC nozzles are based on axisymmetric RANS calculations [2]&[4]. Although Deck et al. [5] performed 3D computations of RSS flow regime in TOC nozzle but their study was concerned about the calculation of side-loads generates in the nozzle due to this separation. Nevertheless three-dimensional simulations are needed to understand the RSS flow regime with special attention on the cap-shock pattern.

In this present study three dimensional numerical investigation of restricted shock separated flow is done to understand the physics of cap-shock pattern. Simulations are performed on a thrust optimized contoured nozzle investigated at Laboratoire d'Études Aérodynamiques (LEA) Poitiers, France, and is denoted as LEATOC nozzle [6]. This flow configurations (restricted shock separation) exhibit massive separation downstream of the nozzle, which makes them well suited for DES. Hence a new version of Detached Eddy Simulation (DES) based on two-equation $k-\omega$ model [12] has been used here, which deals very well with the strong shock wave / boundary layer interaction. Besides a fifth order monotonicity preserving weighted essentially non-oscillatory (MPWENO) [9] numerical scheme is used to achieve high accuracy results in such a complex flow where low order dissipative schemes are not efficient enough.

2 Numerical Methods

The flow configuration considered is a convergent-divergent Thrust-Optimized Contoured (TOC) nozzle. Numerical study on this nozzle has been performed by using the TGNS3D code developed at CEAT/LEA (Poitiers, France). This code solves the three dimensional unsteady compressible Navier-Stokes equations on multiblock structured grid. The Navier-Stokes equations are discretized in space by using a cell centered finite volume method. Restricted shock separated flow is a very complex flow contains a number of flow discontinuities and requires high order numerical scheme with low dissipation for flow analysis. Hence a fifth order Mononicity Preserving Weighted Essentially Non-Oscillatory (MPWENO) scheme [9]. The MPWENO schemes have high phase accuracy and high order of accuracy. The high-order members of this family are almost spectrally accurate for smooth problems. Nevertheless, they have robust shock capturing ability. The flux components assume different values based on the form of the low-order numerical flux that one wishes to employ as a building block for the higher-order WENO flux. They also depend on the order of accuracy of the interpolation. It is shown by Shu and Osher [14], that the higher-order extensions of the ENO schemes built by using the Local Lax-Friedrich (LLF) flux splitting as a building block is only marginally more dissipative than the corresponding ENO schemes that use Roe Flux (RF) as a building block. The first-order RF flux has been found useful in time-dependent problems as a low-order building block for a higher order scheme. One should remember that the RF flux simply utilizes the LLF flux when an entropy fix is desired and reduces to a Roe [15] flux when an entropy fix is not needed. For time integration explicit schemes are not efficient enough for such type of high accelerating flow simulations and an implicit approach is suitable for such cases. A second order two step implicit scheme has been implemented for time discretization. Diagonally dominant alternating direction implicit (DDADI) approach has been used for the inversion of a large sparse matrix system for the implicit scheme. The computational domain is divided into two zones, (i) nozzle and (ii) exterior. The exterior domain extended up to 8 times the nozzle exit radius in the longitudinal direction, and twice in the radial direction (see fig. 1). Based on a previous grid convergence study [7], the optimized reference grid is composed of 2 blocks, 160*100 nodes in the nozzle and 80*160 nodes in the outer zone. The 3D grid is then obtained by rotating this 2D grid every 10^o around the nozzle axis. The value of dimensionless distance $y^+ = (\sqrt{\rho_w|\tau_w|/\mu_w})y = (yu_\tau/\nu_w)$ at the first mesh point on the nozzle wall was calculated and remains less than 0.5, which is quite sufficient for the correct calculation of the viscous stresses.

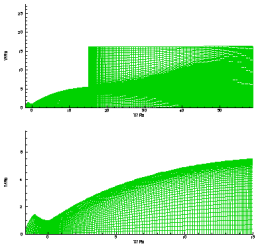

FIG. 1 – Mesh of the computational domain

3 Turbulence Modelling

Number of turbulence models has been proposed for such type of separated flows and few of them have been widely accepted [5],[7]&[8]. Here we have used the $k-\omega$ model as a building block for this DES because of its known ability to predict pressure gradient flows with the success of some of its variants to predict flow separation in other cases. So, a Wilcox standard $k-\omega$ RANS model [12] has been used with the realizability correction proposed by Moore & Moore [11] to enforces the realizability constraint, which common two-equation models violate in strong shock-boundary layer interaction in the outer part of the boundary layer and outside [10]. Than the DES extension of this above realizable model has been done and known as RDES (Realizable DES) which is explained as follows :

3.1 Realizable Detached Eddy Simulation (RDES)

For Wilcox standard $k-\omega$ model, the transport equations of turbulence kinetic energy (k) and specific dissipation (ω) are given below, omitting the density weighted averaging symbols ;

$$\frac{\partial k}{\partial t} + \frac{\partial}{\partial x_j}(kU_j) = P_k - C_{\omega 2}k\omega + \frac{\partial}{\partial x_j}\left((\nu + \frac{\nu_t}{\sigma_k})\frac{\partial k}{\partial x_j}\right) \quad (1)$$

$$\frac{\partial \omega}{\partial t} + \frac{\partial}{\partial x_j}(\omega U_j) = C_{\omega 1}\frac{\omega}{k}P_k - C_{\omega 2}\omega^2 + \frac{\partial}{\partial x_j}\left((\nu + \frac{\nu_t}{\sigma_\omega})\frac{\partial \omega}{\partial x_j}\right) \quad (2)$$

and kinematic eddy viscosity is :

$$\nu_t = k/\omega \quad (3)$$

Where the production term, the stress tensor are respectively given by

$$P_k = \nu_t S^{*2}, \;\; S^* = \sqrt{2S_{ij}S_{ij}}, \;\; S_{ij} = \frac{1}{2}(\frac{\partial u_i}{\partial x_j} + \frac{\partial u_j}{\partial x_i})$$

The standard model constants are retained and are given by :

$$C_{\omega 1} = 5/9, \quad C_{\omega 2} = 3/40, \quad C_\mu = 0.09, \quad \sigma_k = \sigma_\omega = 2$$

In the case of strong interactions a common two-equation turbulence models lead to violate the realizability constraint [10]. The size of the unrealizable zones increases with the interaction strength and they are clearly related to the largest values of the dimensionless strain rate invariant in the flow, especially across the shocks. Following [11], the realizability constraints of two equation models may be enforced by limiting the level of eddy viscosity :

$$\mu_t = \alpha_\nu \rho k/\omega \tag{4}$$

where

$$\alpha_\nu = min(1, \overline{\alpha}_\nu) \quad \& \quad \frac{1}{\overline{\alpha}_\nu} = A_o + A_s(s^2 + A_r\overline{\omega}^2)^{1/2}$$

Here s is the dimensionless mean strain rate S/ω with $S^2 = 2S_{ij}S_{ij} - \frac{1}{2}S_{kk}^2$, and $\overline{\omega}$ is the dimensionless vorticity invariant $\sqrt{2\Omega_{ij}\Omega_{ij}}/\omega$.

$$S_{ij} = \frac{1}{2}\left(\frac{\partial u_i}{\partial x_j} + \frac{\partial u_j}{\partial x_i}\right); \Omega_{ij} = \frac{1}{2}\left(\frac{\partial u_i}{\partial x_j} - \frac{\partial u_j}{\partial x_i}\right) \tag{5}$$

$A_o = 2.85 \; ; \; A_s = 1.77 \; ; \; A_r = 1$

In 2005, J. Yan et al. [13] have investigated different length scales substitutions in DES based on Wilcox standard $k-\omega$ model. Following this, we propose the implementation of DES based on the standard Wilcox $k-\omega$ model with realizability correction. In order to understand the expression of the modifications, equations (1) and (3) are rewritten as follows :

$$\frac{\partial k}{\partial t} + \frac{\partial}{\partial x_j}(kU_j) = P_k - \frac{k^{3/2}}{L_k}\omega + \frac{\partial}{\partial x_j}\left((\nu + \frac{\nu_t}{\sigma_k})\frac{\partial k}{\partial x_j}\right) \tag{6}$$

$$\nu_t = \alpha_\nu C_\mu L_\nu k^{1/2} \tag{7}$$

Here, L_k and L_ν have no independent meaning, but denote the turbulent length scale L_t in equations (4) and (5), respectively. This is defined as

$$L_t = \frac{k^{1/2}}{C_\mu \omega} \tag{8}$$

Within this framework, the length scale introduced is

$$L_{DES} = min(L_t, C_{DES}\Delta) \tag{9}$$

Where C_{DES} is 0.7 [13] and $\Delta = max(\Delta_x, \Delta_y, \Delta_z)$ is the computational mesh size. L_{DES} is a continuous function, given by the minimum of the two length scales. For DES implementation, the turbulent length scale L_t in the dissipation term of k transport equation is replaced by the DES length scale L_{DES}, so that :

$$L_k = L_{DES}, \quad L_\nu = L_t \tag{10}$$

This substitution leads to calculate the eddy viscosity like in the standard RANS model with the realizability correction as discussed earlier.

4 Phenomenology of the Saparated Flow in Rocket Nozzle

An adverse pressure gradient of sufficient strength can cause the boundary layer to separate. Such a condition typically occurs in a nozzle with overexpanded condition, i.e. n (ratio of nozzle exit pressure to the ambient pressure)<1. As soon as n is slightly reduced below one, an oblique shock system is formed from the trailing edge of the nozzle wall due to the induced adverse pressure gradient. When the n is further reduced, to about 0.4-0.8, the viscous layer cannot sustain the adverse gradient imposed upon it by the inviscid flow and the boundary layer separates from the wall. Past research has made it clear that two different separation patterns exist : the classical free shock separation (FSS) and the restricted shock separation (RSS) [1] (see fig. 2).

In the free shock separation case, the overexpanded flow fully separates from the wall. The resulting streamwise wall pressure evolution is mainly governed by the physics of the shock wave/boundary layer interaction occurring in any supersonic flow separation. The separation and the subsequent formation of a recirculation zone give rise to an oblique shock wave near the wall as depicted in fig. 2(left). This incident oblique shock (iS) interacts with the Mach disk (MD), and a reflected shock (rS) appears from the triple point (TP). Due to this oblique shock, the wall pressure suddenly rises and reaches a plateau. Downstream of this plateau, the wall pressure increases slowly up to a level close to the ambient pressure. The separated flow then continues as a free jet. The fluid outside of nozzle gets sucked into it and separates from the nozzle lip, yielding a recirculation bubble counter-rotating with respect to the massively recirculation zone. The exhaust jet flow is delimited by a mixing layer through a channel. This mixing layer can be considered as a "fluid wall" in which the supersonic jet is confined.

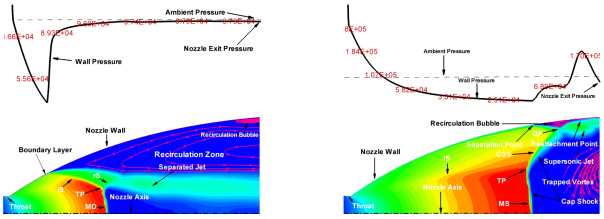

FIG. 2 – (Left) Free shock separation (FSS) ; (Right) Restricted shock separation (RSS)

However, certain circumstances might lead to a reattachment of the flow and hence to a totally different flow pattern called restricted shock separation (see fig. 2(left)). In TOC type rocket nozzles an internal shock (IS) arises in the throat region, where a circular arc forming the nozzle throat turns into the further expansion contour. At this point, wall contour and the wall slope are both continuous, whereas the wall curvature is discontinuous. This eventually generates compression waves coalescing into an internal shock (IS). This internal shock interacts with the small normal shock far away from the throat. In fact, a triple point exists, where the internal shock, the small normal shock and the cone-shaped oblique shock (CSS) meet, indicating a connection between the internal shock and the existence of a cap shock (CS). The incident shock interacts with the cone-shaped oblique shock. Two reflected oblique shocks form from the interaction point, called quadruple point (QP). A free shear layer and the separated boundary layer also interact with these reflected oblique shocks and consequently form two expansion waves. Downstream of interaction, the boundary layer reflects back towards the nozzle wall, reattaches a small recirculation zone attached to the wall. Downstream of the cap-shock a stabilized vortex is trapped quilt by the supersonic jet around it.
In free shock separated flow due to the separation wall pressure rises to the plateau pressure and remains less than the ambient pressure. While in RSS, because of the reattachment and the successive interaction of shock wave and expansion fan in the supersonic jet sudden increase (higher than the ambient pressure) and decrease in pressure takes place (shown in fig. 2).

5 Results and Discussion

Detached eddy simulation of restricted shock separated flow configuration has been performed on LEATOC nozzle. Experimentally it has been found that in LEATOC nozzle RSS flow regimes occurs at relatively high nozzle pressure ratio (i.e. NPR $\geq$ 24).

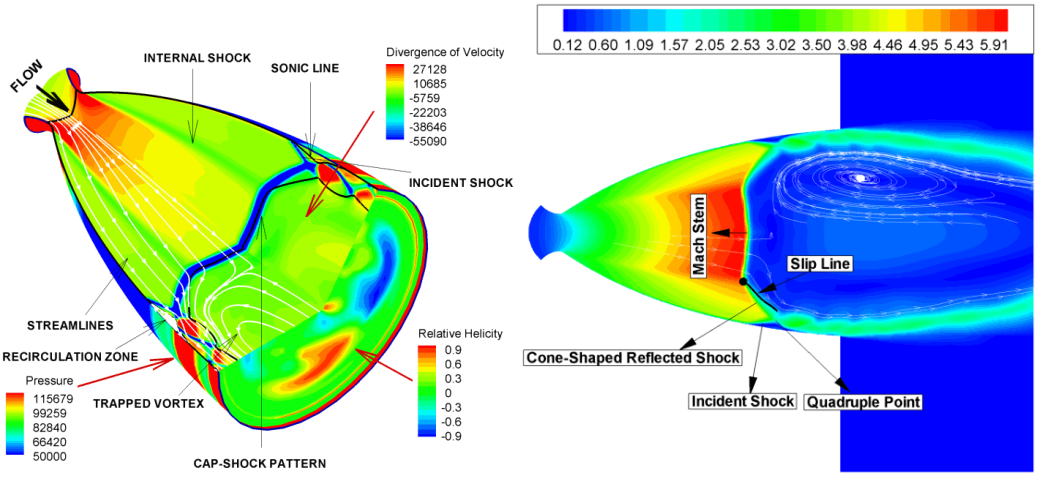

FIG. 3 – (Left) Iso-metric view & (Right) 2D slice of restricted shock separated flow regime.

We have successfully reproduced RSS flow regime at NPR=38, shown in fig. 3. Internal shocks and other flow discontinuities shown in fig. 3(left) are detected with the help iso-velocity divergence contours for this complex flow. The internal shock that appears near the throat region interacts with the Mach stem further downstream of the throat and forms a cone-shaped oblique shock wave. The slip line originates from this triple point is shown in fig. 3(right). Streamlines are drawn on the iso-Mach contours to see the behaviour of the flow after this interaction. One can notice that this slip line is inclined away from the nozzle axis and divert the flow direction towards the nozzle wall. Free shear layer interact with one of the reflected oblique shock from the quadruple point and consequently forms an expansion fan (see fig. 3). Downstream of the interaction the shear later reflect back towards the nozzle axis and surrounds the recirculation zones appears downstream of the cap-shock pattern. This is an adverse pressure gradient trapped vortex stabilized by the supersonic jet around it. The clockwise and anti-clockwise rotation of the trapped vortex is shown by the positive and negative iso-helicity contours (normalized by its maximum value) respectively at the nozzle exit. Iso-pressure contours on the nozzle wall are shown in fig. 3(left), we see the sudden rise in the pressure at the separation point location reaches to the plateau pressure. In the recirculation zone attached to the wall, the pressure remains constant. Again a sudden rise in the wall pressure (higher than the ambient pressure) can be observed at the reattachment point. Successive interactions of shock wave and expansion fan which takes place in the attached supersonic jet cause the increase and decrease in the wall pressure downstream of the reattachment point.

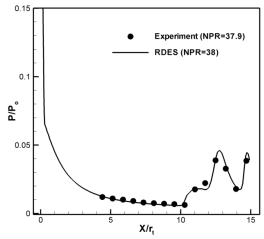

FIG. 4 – Evolution of mean nozzle wall pressure

Numerically obtained mean wall pressure is compared with the available experimental data. This NPR ratio (i.e. 38) is relatively high as compare to the NPR at which FSS flow regime appears (i.e. NPR < 24) in LEATOC nozzle and exhibits strong shock wave / boundary layer interactions. In fig. 4, nozzle mean wall pressure (p) normalized with the inlet total pressure (p_0) has been plotted along the axial direction normalized with the throat radius (r_t) for experimental and numerical data. One can notice that numerically predicted mean separation point and the pressure downstream of it are in excellent agreement with the experimental data. This shows that even at high NPR this DES ensures the realizability constraints.
Although there exist an internal shock at low NPR's in TOC type nozzle and no such RSS flow regime has been seen. To check out the possible causes for the appearance of RSS flow regime mean radial momentum has been plotted for these flow regimes with respect to their Mach stem location, i.e. MS (Mach stem) $\pm\Delta x/r_t$. Here the value of $\Delta x/r_t = 0.65$ has been chosen carefully so that one can take into account the effects caused by the cone-shaped oblique shock. Figure. 5(left) shows the evolution of mean radial momentum along the radial axis of the nozzle for FSS and RSS regimes. In FSS flow configuration Mach disk is located downstream of the separation point. The size of the incident shock is relatively larger than that of the reflected oblique shock and we see the negative momentum (i.e. towards the nozzle axis) before the Mach disk. Due to flow separation a massive recirculation zone appears which in addition to the incident oblique shock produces the radial momentum of sufficient strength that restrains the separated supersonic jet to reattach back to the nozzle wall (see fig. 5(left)). Whereas in RSS flow configuration cone-shaped shock is formed as a result of inverse Mach reflection of the internal shock with the Mach stem, which is located relatively close to the separation point as compare to the FSS case. Downstream of the cone-shaped shock flow is diverted towards the nozzle wall and produces relatively large magnitude of radial momentum towards the nozzle wall. Meanwhile it is

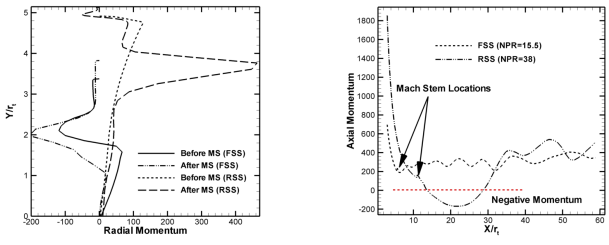

FIG. 5 – (Left) Evolution of Radial & (Right) Axial momentum

noticed that the pressure on the nozzle axis also rises with the increasing x-direction downstream of the cap-shock and produces a force against the main flow. During this phenomenon the strength of the small Mach stem decreases in the radial direction from nozzle axis to the triple point and according to the Crocco's theorem

vorticity is induced behind central part of the cap-shock pattern [16]. It is also found that the size of this recirculation zone increases behind the cap-shock pattern up to 1.5 times the nozzle exit diameter. With the increase in this recirculation zone mean radial momentum away from the nozzle axis is increases. Finally the overall radial momentum becomes sufficient enough to reattach the separated supersonic jet.
Evolution of the axial momentum along the nozzle axis for these flow regimes is also shown in fig. 5 (right). The recirculation zone downstream of the cap-shock pattern (in RSS flow regime) generates a negative momentum along the nozzle axis. This negative axial momentum produces a push against the main flow on the central part of the cap shock and as a consequence the separation point moves further downstream. Furthermore the size of the cone-shaped oblique shock relatively increases (see fig. 3) which give rise to the radial momentum towards the nozzle wall. Whereas in the case of FSS flow configuration no such negative axial momentum has been observed.

6 Conclusions

Three dimensional numerical investigation of a LEATOC nozzle has been performed to understand the complex restricted shock separated flow. A cone-shaped oblique shock is formed due to the inverse Mach reflection of the internal shock with the Mach stem. Downstream of this cone-shaped shock radial momentum away from the nozzle axis is generated. This momentum further increases when the recirculation zone behind the cap-shock pattern appears and produces the negative axial momentum. Hence the mean radial momentum downstream of the cap-shock pattern becomes sufficient enough to reattach the separated supersonic jet. In short nut, one may conclude that cap-shock pattern is the main cause for that restricted shock separated (RSS) flow.

Références

[1] Nave L.H. & Coffey G.A. Sea-level side-load phenomenon in high area ratio rocket engines. 9^{th} Propulsion Conference, AIAA Paper 73-1284, 1973.

[2] Frey M. & Hagemann G. Restricted Shock Separation in rocket nozzles. Journal of Propulsion and Power, Volume 16, No. 3, May-June, 2000.

[3] Nguyen A.T. Découlement instationaire et charges latérales dans les tuyéres propulsives. Ph.D Thesis, Université de Poitiers, 2003.

[4] Hagemann G., Frey M. & Koschel W. Appearance of restricted shock separation in rocket nozzles. Journal of Propulsion and Power, Volume 18, No. 3, May-June, 2002.

[5] Deck S., Garnier E. & Guillen P. Turbulence modelling applied to space launcher configurations. J. of Turbulence, 3 (2002) 057, 2002.

[6] Girard S., Deniau H., Nguyen A.T. & Alziary de Roquefort T. Etude de l'écoulement dans une tuyère propulsive à contour parabolique en régime surdétendu. 37^{eme} Colloque d'Aérodynamique Appliquée de l'AAAF : Aérodynamqieu et Propulsion des Véhicules à grande vitesse, Aracachon, France, 2001.

[7] Shams A., Comte P. Numerical simulation of supersonic overexpanded nozzle. 6th International Bhurban Conference on Applied Sciences & Technology (IBCAST) Islamabad, Pakistan, 2009.

[8] Shams A., Comte P., Girard S., Lehnasch G. & Shahab M.F. 3D Unsteady Numerical Investigation of an Overexpanded Thrust Optimized Contour Nozzle. Sixth European Symposium on Aerothermodynamics for Space Vehicles, Versaille, France, 2008.

[9] Balsara D. S. & Shu C. W. Monotonicity preserving weighted essentially non-oscillatory schemes with increasing high order of accuracy. J. of Computational Physics, Volume 160, Pages 405-452, 2000.

[10] Thivet F., Knight D.D., Zheltovodov A.A. & Maksimov A.I. Some insights in turbulence modeling for crossing shock-wave/boundary-layer interactions. 38^{th} Aerospace Science Meeting & Exhibit, AIAA Paper 2000-0131, 2000.

[11] Moore J.G & Moore J. Realizability in two equation models. 30^{th} Fluid Dynamics Conference, AIAA Paper 99-3779, 1999.

[12] Wilcox D.C. Reassessment of the scale deterring equation for advanced turbulence models. AIAA J. 26 (1988) 1299-1310, 1988.

[13] Yan J., Mockett C. & Thiele F. Investigation of Alternative Length Scale Substitutions in Detached-Eddy Simulation. Flow, Turbulence and Combustion, 74, pp. 85-102, 2005.

[14] Shu W-C., Osher S.J. Efficient implementation of essentially non-oscillatory shock capturing schemes. J. of Computational Physics, 77, 439, 1988.

[15] Roe P.R. Approximate Riemann solvers, parameter vectors, and different schemes. J. of Computational Physics. 43, 357, 1981.

[16] G. Emanuel. Gasdynamics : Theory and Applications, AIAA Education Series, AIAA New York, 1986.